

# Design of Self-supporting Surfaces

## Abstract

Self-supporting masonry is one of the most ancient and elegant techniques for building curved shapes. Because of the very geometric nature of their failure, analyzing and modeling such structures is more a geometry processing problem than one of classical continuum mechanics. In this paper we use the thrust network method of analysis and present an iterative nonlinear optimization algorithm for efficiently approximating freeform shapes by self-supporting ones. Inspired by the rich geometry of thrust networks, initially explored by Maxwell in the 1860s, we establish close connections between different topics of discrete differential geometry, such as a finite-element discretization of the Airy stress potential, perfect graph Laplacians, and the problem of computing admissible loads via curvatures of polyhedral surfaces. This geometric viewpoint allows us, in particular, to remesh self-supporting shapes by self-supporting quad meshes with planar faces.

**CR Categories:** I.3.5 [Computer Graphics]: Computational Geometry and Object Modeling—Curve, surface, solid, and object representations;

**Keywords:** Discrete differential geometry, architectural geometry, self-supporting masonry, thrust networks, reciprocal force diagrams, discrete Laplace operators, isotropic geometry, mean curvature

## 1 Introduction

Vaulted masonry structures are among the simplest and at the same time most elegant solutions for creating curved shapes in building construction. For this reason they have been an object of interest since antiquity; large, non-convex examples of such structures include gothic cathedrals. They continue to be an active topic of research in today's engineering community.

Our paper is concerned with a combined geometry+statics analysis of *self-supporting* masonry and with tools for the interactive modeling of freeform self-supporting structures. Here “self-supporting” means that the structure, considered as an arrangement of blocks (bricks, stones), holds together by itself, with additional support present only during construction. Our analysis is based on the following assumptions, which follow the classic [Heyman 1966]:

*Assumption 1:* Masonry has no tensile strength, but the individual building blocks do not slip against each other (because of friction or mortar). On the other hand, their compressive strength is sufficiently high so that failure of the structure is by a sudden change in geometry and not by material failure.

*Assumption 2 (The Safe Theorem):* If a system of forces can be found which is in equilibrium with the load on the structure and which is contained within the masonry envelope then the structure will carry the loads, although the actual forces present may not be those postulated.

Our approach is twofold: We first give an overview of the continuous case of a smooth surface under stress, which turns out to be governed locally by the so-called Airy stress function. This mathematical model is called a membrane in the engineering literature and has been applied to the analysis of masonry before. The surface is

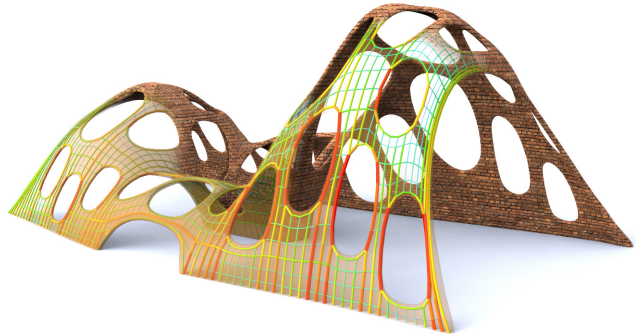


**Figure 1:** A surface with irregularly placed holes almost never stands by itself when built from bricks; for those that do, stability is not obvious by inspection. The surface shown is produced by finding the nearest self-supporting shape from a given freeform geometry. The image also illustrates the fictitious thrust network used in our algorithm, with edges' cross-section and coloring visualizing the magnitude of forces.

self-supporting if and only if stresses are entirely compressive (i.e., the Airy function is convex). For computational purposes, stresses are discretized as a fictitious *thrust network* [Block and Ochsendorf 2007] contained in the masonry structure; this network is a system of forces in equilibrium with the structure's deadload. It can be interpreted as a finite element discretization of the continuous case, and it turns out to have very interesting geometry, with the Airy stress function becoming a polyhedral surface directly related to a reciprocal force diagram.

While previous work in architectural geometry was mostly concerned with aspects of rationalization and purely geometric side-conditions which occur in freeform architecture, the focus of this paper is design with *statics* constraints. In particular, our contributions are the following:

### Contributions.

- We connect the physics of self-supporting surfaces with vertical loads to the geometry of isotropic 3-space, with the direction of gravity as the distinguished direction (§2.3). Taking the convex Airy potential as unit sphere, one can express the equations governing self-supporting surfaces in terms of curvatures.
- We employ Maxwell's construction of polyhedral thrust networks and their reciprocal diagrams (§2.4), and give an interpretation of the equilibrium conditions in terms of discrete curvatures.
- The graph Laplacian derived from a thrust network with compressive forces is a “perfect” one (§2.2). We show how it appears in the analysis and establish a connection with mean curvatures which are otherwise defined for polyhedral surfaces.
- We present an optimization algorithm for efficiently finding a thrust network near a given arbitrary reference surface (§3), and build a tool for interactive design of self-supporting surfaces based on this algorithm (§4).
- We exploit the geometric relationships between a self-supporting surface and its stress potential in order to find particularly nice families of self-supporting surfaces, especially planar quadrilateral representations of thrust networks (§5).

- 88 • We demonstrate the versatility and applicability of our approach  
 89 to the design and analysis of large-scale masonry and steel-glass  
 90 structures.

91 **Related Work.** Unsupported masonry has been an active topic of  
 92 research in the engineering community. The foundations for the  
 93 modern approach were laid by Jacques Heyman [1966] and are  
 94 available as the textbook [Heyman 1995]. The theory of reciprocal  
 95 force diagrams in the planar case was studied by Maxwell [Maxwell  
 96 1864]; a unifying view on polyhedral surfaces, compressive forces  
 97 and corresponding “convex” force diagrams is presented by [Ash  
 98 et al. 1988]. F. Fraternali [2002], [2010] established a connection  
 99 between the continuous theory of stresses in membranes and the  
 100 discrete theory of forces in thrust networks, by interpreting the lat-  
 101 ter as a certain non-conforming finite element discretization of the  
 102 former.

103 Several authors have studied the problem of finding discrete com-  
 104 pressive force networks contained within the boundary of masonry  
 105 structures; previous work in this area includes [O’Dwyer 1998]  
 106 and [Andreu et al. 2007]. Fraternali [2010] proposed solving for  
 107 the structure’s discrete stress surface, and examining its convex  
 108 hull to study the structure’s stability and susceptibility to cracking.  
 109 Philippe Block’s seminal thesis introduced *Thrust Network Analy-  
 110 sis*, which pioneered the use of thrust networks and their reciprocal  
 111 diagrams for efficient and practical design of self-supporting mason-  
 112 ry structures. By first seeking a reciprocal diagram of the top  
 113 view, guaranteeing equilibrium of horizontal forces, then solving  
 114 for the heights that balance the vertical loads, Thrust Network Analy-  
 115 sis linearizes the form-finding problem. For a thorough overview  
 116 of this methodology, see e.g. [Block and Ochsendorf 2007; Block  
 117 2009]. Recent work by Block and coauthors extends this method  
 118 in the case where the reciprocal diagram is not unique; for different  
 119 choices of reciprocal diagram, the optimal heights can be found us-  
 120 ing the method of least squares [Van Mele and Block 2011], and the  
 121 search for the best such reciprocal diagram can be automated using  
 122 a genetic algorithm [Block and Lachauer 2011].

123 Other approaches to the interactive design of self-supporting struc-  
 124 tures include modeling these structures as damped particle-spring  
 125 systems [Kilian and Ochsendorf 2005; Barnes 2009], and mirroring  
 126 the rich tradition in architecture of designing self-supporting  
 127 surfaces using hanging chain models [Heyman 1998]. Alterna-  
 128 tively, masonry structures can be represented by networks of rigid  
 129 blocks [Livesley 1992], whose conditions on the structural feasibil-  
 130 ity were incorporated into procedural modeling of buildings [Whit-  
 131 ing et al. 2009].

132 Algorithmic and mathematical methods relevant to this paper are  
 133 work on the geometry of quad meshes with planar faces [Glymph  
 134 et al. 2004; Liu et al. 2006], discrete curvatures for such meshes  
 135 [Pottmann et al. 2007; Bobenko et al. 2010], in particular curva-  
 136 tures in isotropic geometry [Pottmann and Liu 2007]. Schiftner and  
 137 Balzer [2010] discuss approximating a reference surface by a quad  
 138 mesh with planar faces, whose layout is guided by statics properties  
 139 of that surface.

## 2 Self-supporting Surfaces

### 2.1 The Continuous Theory

142 In this paper we model masonry as a surface given by a height field  
 143  $s(x, y)$  defined in some planar domain  $\Omega$ . We assume that there are  
 144 vertical loads  $F(x, y)$  — usually  $F$  represents the structure’s own  
 145 weight. By definition this surface is self-supporting if and only if  
 146 there exists a field of compressive stresses which are in equilibrium  
 147 with the acting forces. This is equivalent to existence of a field

148  $M(x, y)$  of  $2 \times 2$  symmetric positive semidefinite matrices satisfy-  
 149 ing

$$\operatorname{div}(M\nabla s) = F, \quad \operatorname{div} M = 0, \quad (1)$$

150 where the divergence operator  $\operatorname{div} \begin{pmatrix} u(x, y) \\ v(x, y) \end{pmatrix} = u_x + v_y$  is under-  
 151 stood to act on the columns of a matrix (see e.g. [Fraternali 2010],  
 152 [Giaquinta and Giusti 1985]).

153 The condition  $\operatorname{div} M = 0$  says that  $M$  is locally the Hessian of a  
 154 real-valued function  $\phi$  (the *Airy stress potential*): With the notation

$$M = \begin{pmatrix} m_{11} & m_{12} \\ m_{12} & m_{22} \end{pmatrix} \iff \widehat{M} = \begin{pmatrix} m_{22} & -m_{12} \\ -m_{12} & m_{11} \end{pmatrix}$$

155 it is clear that  $\operatorname{div} M = 0$  is an integrability condition for  $\widehat{M}$ , so  
 156 locally there is a potential  $\phi$  with

$$\widehat{M} = \nabla^2 \phi, \quad \text{i.e.,} \quad M = \widehat{\nabla^2 \phi}.$$

157 If the domain  $\Omega$  is simply connected, this relation holds globally.  
 158 Positive semidefiniteness of  $M$  (or equivalently of  $\widehat{M}$ ) character-  
 159 izes *convexity* of the Airy potential  $\phi$ . The Airy function enters  
 160 computations only by way of its derivatives, so global existence is  
 161 not an issue.

162 *Remark:* Stresses at boundary points depend on the way the sur-  
 163 face is anchored: A fixed anchor means no condition, but a free  
 164 boundary with outer normal vector  $\mathbf{n}$  means  $\langle M\nabla s, \mathbf{n} \rangle = 0$ .

165 **Stress Laplacian.** Note that  $\operatorname{div} M = 0$  yields  $\operatorname{div}(M\nabla s) =$   
 166  $\operatorname{tr}(M\nabla^2 s)$ , which we like to call  $\Delta_\phi s$ . The operator  $\Delta_\phi$  is sym-  
 167 metric. It is elliptic (as a Laplace operator should be) if and only if  
 168  $M$  is positive definite, i.e.,  $\phi$  is strictly convex. The balance condi-  
 169 tion (1) may be written as  $\Delta_\phi s = F$ .

### 2.2 Discrete Theory: Thrust Networks

170 We discretize a self-supporting surface by a mesh  $\mathcal{S} = (V, E, F)$   
 171 (see Figure 2). Loads are again vertical, and we discretize them as  
 172 force densities  $F_i$  associated with vertices  $\mathbf{v}_i$ . The load acting on  
 173 this vertex is then given by  $F_i A_i$ , where  $A_i$  is an area of influence  
 174 (using a prime to indicate projection onto the  $xy$  plane,  $A_i$  is the  
 175 area of the Voronoi cell of  $\mathbf{v}'_i$  w.r.t.  $V'$ ). We assume that stresses  
 176 are carried by the edges of the mesh: the force exerted on the vertex  
 177  $\mathbf{v}_i$  by the edge connecting  $\mathbf{v}_i, \mathbf{v}_j$  is given by

$$w_{ij}(\mathbf{v}_j - \mathbf{v}_i), \quad \text{where } w_{ij} = w_{ji} \geq 0.$$

178 The nonnegativity of the individual weights  $w_{ij}$  expresses the com-  
 179 pressive nature of forces. The balance conditions at vertices then  
 180 read as follows: With  $\mathbf{v}_i = (x_i, y_i, s_i)$  we have

$$\sum_{j \sim i} w_{ij}(x_j - x_i) = \sum_{j \sim i} w_{ij}(y_j - y_i) = 0, \quad (2)$$

$$\sum_{j \sim i} w_{ij}(s_j - s_i) = A_i F_i. \quad (3)$$

182 A mesh equipped with edge weights in this way is a discrete *thrust*  
 183 *network*. Invoking the safe theorem, we can state that a masonry  
 184 structure is self-supporting, if we can find a thrust network with  
 185 compressive forces which is entirely contained within the structure.

186 **Reciprocal Diagram.** Equations (2) have a geometric interpreta-  
 187 tion: with edge vectors

$$\mathbf{e}'_{ij} = \mathbf{v}'_j - \mathbf{v}'_i = (x_j, y_j) - (x_i, y_i),$$

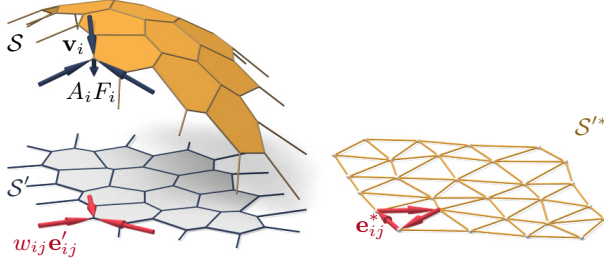


**Figure 2:** A thrust network  $\mathcal{S}$  with dangling edges indicating external forces (left). This network together with compressive forces which balance vertical loads  $A_i F_i$  projects onto a planar mesh  $\mathcal{S}'$  with equilibrium compressive forces  $w_{ij} \mathbf{e}'_{ij}$  in its edges. Rotating forces by  $90^\circ$  leads to the reciprocal force diagram  $\mathcal{S}'^*$  (right).

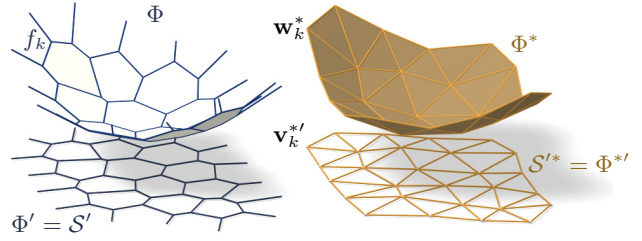


**Figure 3:** Airy stress potential  $\Phi$  and its polar dual  $\Phi^*$ .  $\Phi$  projects onto the same planar mesh as  $\mathcal{S}$  does, while  $\Phi^*$  projects onto the reciprocal force diagram. A primal face  $f_k$  lies in the plane  $z = \alpha x + \beta y + \gamma \iff$  the corresponding dual vertex is  $\mathbf{w}_k^* = (\alpha, \beta, -\gamma)$ .

188 Equation (2) asserts that vectors  $w_{ij} \mathbf{e}'_{ij}$  form a closed cycle. Rotating them by 90 degrees, we see that likewise  
189

$$\mathbf{e}'_{ij}^* = w_{ij} J \mathbf{e}'_{ij}, \quad \text{with } J = \begin{pmatrix} 0 & -1 \\ 1 & 0 \end{pmatrix},$$

190 form a closed cycle (see Figure 2). If the mesh  $\mathcal{S}$  is simply connected, there exists an entire reciprocal diagram  $\mathcal{S}'^*$  which is a  
191 192 combinatorial dual of  $\mathcal{S}$ , and which has edge vectors  $\mathbf{e}'_{ij}^*$ . Its vertices are denoted by  $\mathbf{v}'_i^*$ .  
193

194 *Remark:* If  $\mathcal{S}'$  is a Delaunay triangulation, then the corresponding  
195 Voronoi diagram is an example of a reciprocal diagram.

196 **Polyhedral Stress Potential.** We can go further and construct a  
197 convex polyhedral “Airy stress potential” surface  $\Phi$  with vertices  
198  $\mathbf{w}_i = (x_i, y_i, \phi_i)$  combinatorially equivalent to  $\mathcal{S}$  by requiring that  
199 a primal face of  $\Phi$  lies in the plane  $z = \alpha x + \beta y + \gamma$  if and only if  
200  $(\alpha, \beta)$  is the corresponding dual vertex of  $\mathcal{S}'^*$  (see Figure 3). Ob-  
201 202 viously this condition determines  $\Phi$  up to vertical translation. For  
203 existence see [Ash et al. 1988]. The inverse procedure constructs  
204 a reciprocal diagram from  $\Phi$ . This procedure works also if forces  
205 are not compressive: we can construct an Airy mesh  $\Phi$  which has  
206 planar faces, but it will no longer be a convex polyhedron.

207 The vertices of  $\Phi$  can be interpolated by a piecewise-linear function  
208  $\phi(x, y)$ . It is easy to see that the derivative of  $\phi(x, y)$  jumps by the  
209 amount  $\|\mathbf{e}'_{ij}^*\| = w_{ij} \|\mathbf{e}'_{ij}\|$  when crossing over the edge  $\mathbf{e}'_{ij}$  at right  
210 angle, with unit speed. This identifies  $\Phi$  as the Airy polyhedron in-  
211 212 troduced by [Fraternali et al. 2002] as a finite element discretization  
213 of the continuous Airy function (see also [Fraternali 2010]).

214 If the mesh is not simply connected, the reciprocal diagram and  
215 the Airy polyhedron exist only locally. Our computations do not  
216 require global existence.

217 **Polarity.** Polarity with respect to the *Maxwell paraboloid*  $z =$   
218  $\frac{1}{2}(x^2 + y^2)$  maps the plane  $z = \alpha x + \beta y + \gamma$  to the point  $(\alpha, \beta, -\gamma)$ .  
219 Thus, applying polarity to  $\Phi$  and projecting the result  $\Phi^*$  into the  $xy$   
220 plane reconstructs the reciprocal diagram  $\Phi'^* = \mathcal{S}'^*$  (see Fig. 3).

221 **Discrete Stress Laplacian.** The weights  $w_{ij}$  may be used to de-  
222 fine a graph Laplacian  $\Delta_\phi$  which on vertex-based functions acts as

$$\Delta_\phi s(\mathbf{v}_i) = \sum_{j \sim i} w_{ij} (s_j - s_i).$$

223 This operator is a perfect discrete Laplacian in the sense of [War-  
224 detzky et al. 2007], since it is symmetric by construction, Equa-  
225 tion (2) implies linear precision for the planar “top view mesh”  $\mathcal{S}'$   
226 (i.e.,  $\Delta_\phi f = 0$  if  $f$  is a linear function), and  $w_{ij} \geq 0$  ensures

225 semidefiniteness and a maximum principle for  $\Delta_\phi$ -harmonic func-  
226 tions. Equation (3) can be written as  $\Delta_\phi s = AF$ .

227 Note that  $\Delta_\phi$  is well defined even when the underlying meshes are  
228 not simply connected.

### 2.3 Surfaces in Isotropic Geometry

230 It is worthwhile to reconsider the basics of self-supporting surfaces  
231 in the language of dual-isotropic geometry, which takes place in  $\mathbb{R}^3$   
232 with the  $z$  axis as a distinguished vertical direction. The basic ele-  
233 234 ments of this geometry are planes, having equation  $z = f(x, y) =$   
235  $\alpha x + \beta y + \gamma$ . The gradient vector  $\nabla f = (\alpha, \beta)$  determines the  
236 plane up to translation. A plane tangent to the graph of the function  
237  $s(x, y)$  has gradient vector  $\nabla s$ .

238 There is the notion of *parallel points*:  $(x, y, z) \parallel (x', y', z') \iff$   
239  $x = x', y = y'$ .

240 *Remark:* The Maxwell paraboloid is considered the unit sphere of  
241 isotropic geometry, and the geometric quantities considered above  
242 are assigned specific meanings: The forces  $\|\mathbf{e}'_{ij}\| = w_{ij} \|\mathbf{e}_{ij}\|$  are  
243 dihedral angles of the Airy polyhedron  $\Phi$ , and also “lengths” of  
edges of  $\Phi^*$ . We do not use this terminology in the sequel.

244 **Curvatures.** Generally speaking, in the differential geometry of  
245 surfaces one considers the *Gauss map*  $\sigma$  from a surface  $S$  to a con-  
246 247 vex unit sphere  $\Phi$  by requiring that corresponding points have par-  
248 249 allel tangent planes. Subsequently mean curvature  $H^{\text{rel}}$  and Gaus-  
250 sian curvature  $K^{\text{rel}}$  relative to  $\Phi$  are computed from the derivative  
251  $d\sigma$ . Classically  $\Phi$  is the ordinary unit sphere  $x^2 + y^2 + z^2 = 1$ , so  
252 that  $\sigma$  maps each point its unit normal vector.

253 In our setting, parallelity is a property of *points* rather than planes,  
254 and the Gauss map  $\sigma$  goes the other way, mapping the tangent  
255 planes of the unit sphere  $z = \phi(x, y)$  to the corresponding tan-  
256 257 gent plane of the surface  $z = s(x, y)$ . If we know which point a  
258 plane is attached to, then it is determined by its gradient. So we  
259 simply write

$$\nabla \phi \stackrel{\sigma}{\mapsto} \nabla s.$$

260 By moving along a curve  $\mathbf{u}(t) = (x(t), y(t))$  in the parameter  
261 domain we get the first variation of tangent planes:  $\frac{d}{dt} \nabla \phi|_{\mathbf{u}(t)} =$   
262  $(\nabla^2 \phi) \dot{\mathbf{u}}$ . This yields the derivative  $(\nabla^2 \phi) \dot{\mathbf{u}} \stackrel{d\sigma}{\mapsto} (\nabla^2 s) \dot{\mathbf{u}}$ , for all  
263  $\dot{\mathbf{u}}$ , and the matrix of  $d\sigma$  is found as  $(\nabla^2 \phi)^{-1} (\nabla^2 s)$ . By definition,

261 curvatures of the surface  $s$  relative to  $\phi$  are found as

$$\begin{aligned} K_s^{\text{rel}} &= \det(d\sigma) = \frac{\det \nabla^2 s}{\det \nabla^2 \phi}, \\ H_s^{\text{rel}} &= \frac{1}{2} \text{tr}(d\sigma) = \frac{1}{2} \text{tr} \left( \frac{M}{\det \nabla^2 \phi} \nabla^2 s \right) = \frac{\Delta_\phi s}{2 \det \nabla^2 \phi}. \end{aligned}$$

262 The Maxwell paraboloid  $\phi_0(x, y) = \frac{1}{2}(x^2 + y^2)$  is the canonical  
263 unit sphere of isotropic geometry, with Hessian  $E_2$ . Curvatures relative  
264 to  $\phi_0$  are not called “relative” and are denoted by the symbols  
265  $H, K$  instead of  $H^{\text{rel}}, K^{\text{rel}}$ . The observation

$$\Delta_\phi \phi = \text{tr}(M \nabla^2 \phi) = \text{tr}(\widehat{\nabla^2 \phi} \nabla^2 \phi) = 2 \det \nabla^2 \phi$$

266 together with the formulas above implies

$$K_s = \det \nabla^2 s, \quad K_\phi = \det \nabla^2 \phi \implies H_s^{\text{rel}} = \frac{\Delta_\phi s}{2K_\phi} = \frac{\Delta_\phi s}{\Delta_\phi \phi}.$$

267 **Relation to Self-supporting Surfaces.** Summarizing the for-  
268 mulae above, we rewrite the balance condition (1) as

$$2K_\phi H_s^{\text{rel}} = \Delta_\phi s = F. \quad (4)$$

269 Let us draw some conclusions:

- Since  $H_\phi^{\text{rel}} = 1$  we see that the load  $F_\phi = 2K_\phi$  is admissible for the stress surface  $\phi(x, y)$ , which is hereby shown as self-supporting. The quotient of loads yields  $H_s^{\text{rel}} = F/F_\phi$ .
- If the stress surface coincides with the Maxwell paraboloid, then *constant loads characterize constant mean curvature surfaces*, because we get  $K_\phi = 1$  and  $H_s = F/2$ .
- If  $s_1, s_2$  have the same stress potential  $\phi$ , then  $H_{s_1-s_2}^{\text{rel}} = H_{s_1}^{\text{rel}} - H_{s_2}^{\text{rel}} = 0$ , so  $s_1 - s_2$  is a (relative) minimal surface.

## 2.4 Meshes in Isotropic Geometry

270 A general theory of curvatures of polyhedral surfaces with respect  
271 to a polyhedral unit sphere was proposed by [Pottmann et al. 2007;  
272 Bobenko et al. 2010], and its dual complement in isotropic geo-  
273 metry was elaborated on in [Pottmann and Liu 2007]. As illustrated by  
274 Figure 4, the mean curvature of a self-supporting surface  $S$  relative  
275 to its discrete Airy stress potential is associated with the vertices of  
276  $S$ . It is computed from areas and mixed areas of faces in the polar  
277 polyhedra  $S^*$  and  $\Phi^*$ :

$$H^{\text{rel}}(\mathbf{v}_i) = \frac{A_i(\mathcal{S}, \Phi)}{A_i(\Phi, \Phi)}, \quad \text{where}$$

$$A_i(\mathcal{S}, \Phi) = \frac{1}{4} \sum_{k: f_k \in 1\text{-ring}(\mathbf{v}_i)} \det(\mathbf{v}'_k, \mathbf{w}'_{k+1}) + \det(\mathbf{w}'_k, \mathbf{v}'_{k+1}).$$

287 The prime denotes the projection into the  $xy$  plane, and summation  
288 is over those dual vertices which are adjacent to  $\mathbf{v}_i$ . Replacing  $\mathbf{v}'_k$   
289 by  $\mathbf{w}'_k$  yields  $A_i(\Phi, \Phi) = \frac{1}{2} \sum \det(\mathbf{w}'_k, \mathbf{w}'_{k+1})$ .

290 **Proposition.** If  $\Phi$  is the Airy surface of a thrust network  $\mathcal{S}$ , then  
291 the mean curvature of  $\mathcal{S}$  relative to  $\Phi$  is computable as

$$H^{\text{rel}}(\mathbf{v}_i) = \frac{\sum_{j \sim i} w_{ij}(s_j - s_i)}{\sum_{j \sim i} w_{ij}(\phi_j - \phi_i)} = \frac{\Delta_\phi s}{\Delta_\phi \phi} \Big|_{\mathbf{v}_i}. \quad (5)$$

292 **Proof.** It is sufficient to show  $2A_i(\mathcal{S}, \Phi) = \sum_{j \sim i} w_{ij}(s_j - s_i)$ .

293 For that, consider edges  $\mathbf{e}'_1, \dots, \mathbf{e}'_n$  emanating from  $\mathbf{v}'_i$ . The dual  
294 cycles in  $\Phi^{**}$  and  $\mathcal{S}^{**}$  without loss of generality are given by ver-  
295 tices  $(\mathbf{v}'_1, \dots, \mathbf{v}'_n)$  and  $(\mathbf{w}'_1, \dots, \mathbf{w}'_n)$ , respectively. The latter  
296 has edges  $\mathbf{w}'_{j+1} - \mathbf{w}'_j = w_{ij} J \mathbf{e}'_j$  (indices modulo  $n$ ).

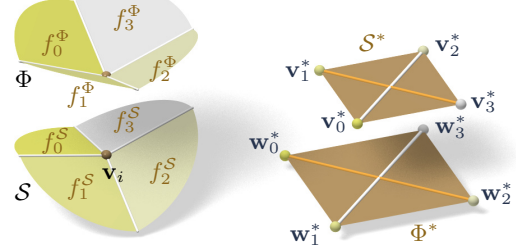


Figure 4: Mean curvature of a vertex  $\mathbf{v}_i$  of  $\mathcal{S}$ : Corresponding edges of the polar duals  $\mathcal{S}^*$ ,  $\Phi^*$  are parallel, and mean curvature according to [Pottmann et al. 2007] is computed from the vertices polar to faces adjacent to  $\mathbf{v}_i$ . For valence 4 vertices the case of zero mean curvature shown here is characterized by parallelity of non-corresponding diagonals of corresponding quads in  $\mathcal{S}^*$ ,  $\Phi^*$ .

297 Without loss of generality  $\mathbf{v}_i = 0$ , so the vertex  $\mathbf{v}'_j$  by construction  
298 equals the gradient of the linear function  $\mathbf{x} \mapsto \langle \mathbf{v}'_j, \mathbf{x} \rangle$  defined by  
299 the properties  $\mathbf{e}'_{j-1} \mapsto s_{j-1} - s_i$ ,  $\mathbf{e}'_j \mapsto s_j - s_i$ . Corresponding  
300 edge vectors  $\mathbf{v}'_{j+1} - \mathbf{v}'_j$  and  $\mathbf{w}'_{j+1} - \mathbf{w}'_j$  are parallel, because  
301  $\langle \mathbf{v}'_{j+1} - \mathbf{v}'_j, \mathbf{e}'_j \rangle = (s_j - s_i) - (s_j - s_i) = 0$ . Expand  $2A_i(\mathcal{S}, \Phi)$ :

$$\begin{aligned} &\frac{1}{2} \sum \det(\mathbf{w}'_j, \mathbf{v}'_{j+1}) + \det(\mathbf{v}'_j, \mathbf{w}'_{j+1}) \\ &= \frac{1}{2} \sum \det(\mathbf{w}'_j - \mathbf{w}'_{j+1}, \mathbf{v}'_{j+1}) + \det(\mathbf{v}'_j, \mathbf{w}'_{j+1} - \mathbf{w}'_j) \\ &= \frac{1}{2} \sum \det(-w_{ij} J \mathbf{e}'_j, \mathbf{v}'_{j+1}) + \det(\mathbf{v}'_j, w_{ij} J \mathbf{e}'_j) \\ &= \sum w_{ij} \langle \mathbf{v}'_j, \mathbf{e}'_j \rangle = \sum w_{ij} (s_j - s_i). \end{aligned}$$

302 Here we have used  $\det(\mathbf{a}, J\mathbf{b}) = \langle \mathbf{a}, \mathbf{b} \rangle$ .  $\square$

303 In order to discretize (4), we also need a discrete Gaussian curva-  
304 ture, usually defined as a quotient of areas which correspond under  
305 the Gauss mapping. We define

$$K_\Phi(\mathbf{v}_i) = \frac{A_i(\Phi, \Phi)}{A_i},$$

306 where  $A_i$  is the Voronoi area of vertex  $\mathbf{v}'_i$  in the projected mesh  $\mathcal{S}'$   
307 used in (3).

308 *Remark:* If the faces of the thrust network  $\mathcal{S}$  are not planar, the sim-  
309 ple trick of introducing additional edges with zero forces in them  
310 makes them planar, and the theory is applicable. In the interest of  
311 space, we refrain from elaborating further.

312 **Discrete Balance Equation.** The discrete version of the balance  
313 equation (4) reads as follows:

314 **Theorem.** A simply-connected mesh  $\mathcal{S}$  with vertices  $\mathbf{v}_i =$   
315  $(x_i, y_i, s_i)$  can be put into static equilibrium with vertical nodal  
316 forces  $A_i F_i$  if and only if there exists a combinatorially equivalent  
317 mesh  $\Phi$  with planar faces and vertices  $(x_i, y_i, \phi_i)$ , such that cur-  
318 vatures of  $\mathcal{S}$  relative to  $\Phi$  obey

$$2K_\Phi(\mathbf{v}_i) H^{\text{rel}}(\mathbf{v}_i) = F_i \quad (6)$$

319 at every interior vertex and every free boundary vertex  $\mathbf{v}_i$ .  $\mathcal{S}$  can  
320 be put into compressive static equilibrium if and only if there exists  
321 a convex such  $\Phi$ .

322 *Proof.* The relation between equilibrium forces  $w_{ij} \mathbf{e}_{ij}$  in  $\mathcal{S}$  and  
323 the polyhedral stress potential  $\Phi$  has been discussed above, and  
324 so has the equivalence “ $w_{ij} \geq 0 \iff \Phi$  convex” (see e.g.  
325 [Ash et al. 1988] for a survey of this and related results). It re-  
326 mains to show that Equations (2) and (6) are equivalent. This is

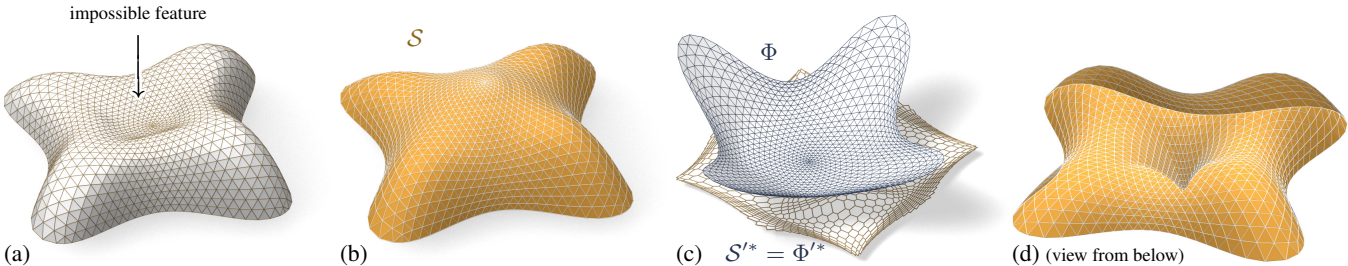


**Figure 5:** The top of the Lilium Tower (a) cannot stand as a masonry structure, because its central part is concave. Our algorithm finds a nearby self-supporting mesh (b) without this impossible feature. (c) shows the corresponding Airy mesh  $\Phi$  and reciprocal force diagram  $S'^*$ . (d) The user can edit the original surface, such as by specifying that the center of the surface is supported by a vertical pillar; and the self-supporting network adjusts accordingly.

327 the case because the proposition above implies  $2K(\mathbf{v}_i)H^{\text{rel}}(\mathbf{v}_i) =$  371  
 328  $2\frac{A_i(\Phi, \Phi)}{A_i} \frac{A_i(\Phi, \mathcal{S})}{A_i(\Phi, \Phi)} = \frac{1}{A_i}(\sum_{j \sim i} w_{ij}(s_j - s_i)) = \frac{1}{A_i} A_i F_i.$  □ 372  
 373

2. Fixing  $\mathcal{S}$ , locally fit an associated stress surface  $\Phi$ .
3. Alter positions  $\mathbf{v}_i$  to improve the fit.
4. Repeat from Step 1 until convergence.

329 **Existence of Discretizations.** When considering discrete thrust  
 330 networks as discretizations of continuous self-supporting surfaces,  
 331 the following question is important: For a given smooth surface  
 332  $s(x, y)$  with Airy stress function  $\phi$ , does there exist a polyhedral  
 333 surface  $\mathcal{S}$  in equilibrium approximating  $s(x, y)$ , whose top view  
 334 is a given planar mesh  $\mathcal{S}'$ ? We restrict our attention to triangle  
 335 meshes, where planarity of the faces of the discrete stress surface  $\Phi$   
 336 is not an issue. This question has several equivalent reformulations:  
 337

- Does  $\mathcal{S}'$  have a reciprocal diagram whose corresponding Airy polyhedron  $\Phi$  approximates the continuous Airy potential  $\phi$ ? (if the surfaces involved are not simply connected, these objects are defined locally).
- Does  $\mathcal{S}'$  possess a “perfect” discrete Laplace-Beltrami operator  $\Delta_\phi$  in the sense of Wardetzky et al. [2007] whose weights are the edge length scalars of such a reciprocal diagram?

344 From [Wardetzky et al. 2007] we know that perfect Laplacians ex-  
 345 ist only on regular triangulations which are projections of convex  
 346 polyhedra. On the other hand, previous sections show how to ap-  
 347 propriately re-triangulate: Let  $\Phi$  be a triangle mesh convex hull of  
 348 the vertices  $(x_i, y_i, \phi(x_i, y_i))$ , where  $(x_i, y_i)$  are vertices of  $\mathcal{S}'$ .  
 349 Then its polar dual  $\Phi^*$  projects onto a reciprocal diagram with pos-  
 350 itive edge weights, so  $\Delta_\phi$  has positive weights, and the vertices  
 351  $(x_i, y_i, s_i)$  of  $\mathcal{S}$  can be found by solving the discrete Poisson prob-  
 352 lem  $(\Delta_\phi s)_i = A_i F_i$ .

353 Assuming the discrete  $\Delta_\phi$  approximates its continuous counter-  
 354 part, this yields a mesh approximating  $s(x, y)$ , and we conclude: A  
 355 *smooth self-supporting surface can be approximated by a discrete*  
 356 *self-supporting triangular mesh for any sampling of the surface.*

374 This staggered approach has several advantages: a nearby self-sup-  
 375 porting surface is found given only a suggested reference shape,  
 376 without needing to single one of the many possible top view re-  
 377 ciprocal diagrams or needing to specify boundary tractions – these  
 378 are found automatically during optimization. Although providing  
 379 an initial top view graph with good combinatorics remains impor-  
 380 tant, our approach allows the thrust network to slide both vertically  
 381 and tangentially to the ground, essential to finding faithful thrust  
 382 networks for surfaces with free boundary conditions. The cheese  
 383 cheese surface 1, for example, relies heavily on such sliding.

384 **Step 1: Estimating Self-Load.** The dead load due to the sur-  
 385 face’s own weight depends not only on the top view of  $\mathcal{S}$ , but also  
 386 on the surface area of its faces. To avoid adding nonlinearity to  
 387 the algorithm, we estimate the load coefficients  $F_i$  at the beginning  
 388 of each iteration, and assume they remain constant until the next  
 389 iteration. We estimate the load  $A_i F_i$  associated with each vertex  
 390 by calculating its Voronoi surface area on each of its incident faces  
 391 (note that this surface area is distinct from  $A_i$ , the vertex’s Voronoi  
 392 area on the top view), and then multiplying by a user-specified sur-  
 393 face density  $\rho$ .

394 **Step 2: Fit a Stress Surface.** In this step, we fix  $\mathcal{S}$  and try to  
 395 fit a stress surface  $\Phi$  subordinate to the top view  $\mathcal{S}'$  of the primal  
 396 mesh. We do so by searching for dihedral angles between the faces  
 397 of  $\Phi$  which minimize, in the least-squares sense, the error in force  
 398 equilibrium (6) and local integrability of  $\Phi$ . Doing so is equivalent  
 399 to minimizing the squared residuals of Equations (3) and (2), re-  
 400 spectively, with the positions held fixed. Defining the *equilibrium*  
 401 *energy*

$$E = \sum_i \left\| \begin{pmatrix} 0 \\ 0 \\ A_i F_i \end{pmatrix} - \sum_{j \sim i} w_{ij} (\mathbf{v}_j - \mathbf{v}_i) \right\|^2, \quad (7)$$

402 where the outer sum is over the interior and free boundary vertices,  
 403 we solve

$$\min_{w_{ij}} E, \quad \text{s.t. } 0 \leq w_{ij} \leq w_{\max}. \quad (8)$$

404 Here  $w_{\max}$  is an optional maximum weight we are willing to assign  
 405 (to limit the amount of stress in the surface). This convex, sparse,  
 406 box-constrained least-squares problem [Friedlander 2007] always  
 407 has a solution. If the objective is 0 at this solution, the faces of  $\Phi$   
 408 locally integrate to a stress surface satisfying (6), and this  $\Phi$  certifies  
 409 that  $\mathcal{S}$  is self-supporting – we are done. Otherwise,  $\mathcal{S}$  is not self-  
 410 supporting and its vertices must be moved.

### 3 Thrust Networks from Reference Meshes

357 Consider now the problem of taking a given reference mesh, say  
 358  $\mathcal{R}$ , and finding a combinatorially equivalent mesh  $\mathcal{S}$  in static equi-  
 359 librium approximating  $\mathcal{R}$ . The loads on  $\mathcal{S}$  include user-prescribed  
 360 loads as well as the dead load caused by the mesh’s own weight.  
 361 Conceptually, finding  $\mathcal{S}$  amounts to minimizing some formulation  
 362 of distance between  $\mathcal{R}$  and  $\mathcal{S}$ , subject to constraints (2), (3), and  
 363  $w_{ij} \geq 0$ . For any choice of distance this minimization will be a  
 364 nonlinear, non-convex, inequality-constrained variational problem  
 365 that cannot be efficiently solved in practice. Instead we propose a  
 366 staggered optimization algorithm:

0. Start with an initial guess  $\mathcal{S} = \mathcal{R}$ .
1. Estimate the self-load on the vertices of  $\mathcal{S}$ , using their current positions.

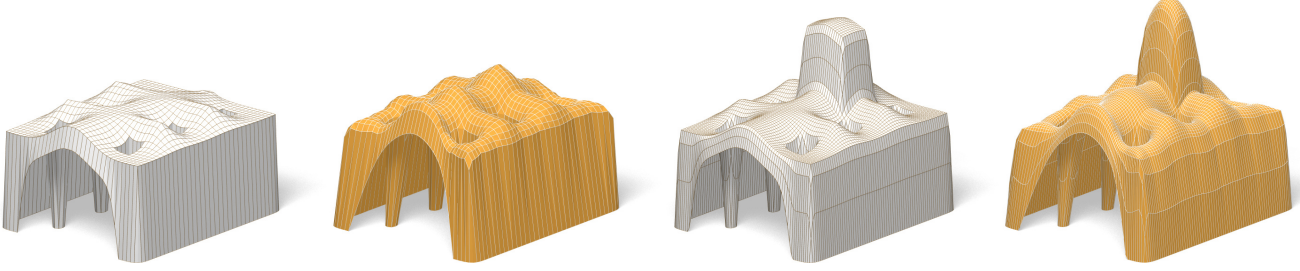


**Figure 6:** The user-designed reference mesh (left) is not self-supporting, but our algorithm finds a nearby perturbation of the reference surface (middle-left) that is in equilibrium. As the user makes edits to the reference surface (middle-right), the thrust network automatically adjusts (right).

Example	Figure	Vertices	Edges	Time (s)	Iterations	Max Rel Error
Top of Lilium Tower	Fig. 5b	1201	3504	21.6	9	$4.2 \times 10^{-5}$
Top of Lilium Tower (with pillar)	Fig. 5d	1200	3500	26.5	10	$8.5 \times 10^{-5}$
Freeform Structure with Two Pillars	Fig. 7	1535	2976	17.0	21	$2.7 \times 10^{-5}$
Swiss Cheese	Fig. 9	2358	4302	19.5	9	$3.0 \times 10^{-4}$
Brick Domes	Fig. 8	752	2165	8.0	9	$5.8 \times 10^{-5}$
Structural Glass	Fig. 15	527	998	5.7	25	$2.4 \times 10^{-5}$

**Table 1:** Numerical details about the examples throughout this paper. Time: The wall-clock time needed by an Intel Xeon 2.3GHz desktop PC with 4 GB of RAM to find a self-supporting thrust network and associated stress surface from the example’s reference mesh; we also give the number of outer iterations of the four steps in (§3). The maximum relative error is the dimensionless relative error in force equilibrium defined by  $\max_i \|A_i F_i - \sum_{j \sim i} w_{ij}(\mathbf{v}_j - \mathbf{v}_i)\| / \|A_i F_i\|$ , where the maximum is taken over interior vertices  $\mathbf{v}_i$ .

411 **Step 3: Alter Positions.** In the previous step we fit as best as  
 412 possible a stress surface  $\Phi$  to  $\mathcal{S}$ . There are two possible kinds of  
 413 error with this fit: the faces around a vertex (equivalently, the recip-  
 414 415 416 417 418 419  
 420 421 422 423 424 425  
 426 427 428 429 430 431 432 433 434 435  
 436 437 438 439 440 441  
 442 443 444 445 446 447  
 448 449 450 451 452 453 454 455 456 457 458  
 459 460 461 462 463 464 465 466 467 468 469  
 470

In the previous step we fit as best as possible a stress surface  $\Phi$  to  $\mathcal{S}$ . There are two possible kinds of error with this fit: the faces around a vertex (equivalently, the reciprocal diagram) might not close up; and the resulting stress forces might not be exactly in equilibrium with the loads. These errors can be decreased by modifying the top view and heights of  $\mathcal{S}$ , respectively. It is possible to simply solve for new vertex positions that put  $\mathcal{S}$  in static equilibrium, since Equations (2) and (3) with  $w_{ij}$  fixed form a square linear system that is typically nonsingular.

While this approach would yield a self-supporting  $\mathcal{S}$ , this mesh is often far from the reference mesh  $\mathcal{R}$ , since any local errors in the stress surface from Step 2 amplify into global errors in  $\mathcal{S}$ . We propose instead to look for new positions that decrease the imbalance in the stresses and loads, while also penalizing drift away from the reference mesh:

$$\min_{\mathbf{v}} E + \alpha \sum_i \langle \mathbf{n}_i, \mathbf{v}_i - \mathbf{v}_i^0 \rangle^2 + \beta \|\mathbf{v} - \mathbf{v}_P^0\|^2,$$

where  $\mathbf{v}_i^0$  is the position of the  $i$ -th vertex at the start of this step of the optimization,  $\mathbf{n}_i$  is the starting vertex normal (computed as the average of the incident face normals),  $\mathbf{v}_P^0$  is the projection of  $\mathbf{v}^0$  onto the reference mesh, and  $\alpha > \beta$  are penalty coefficients that are decreased every iteration of Steps 1–3 of the algorithm. The second term allows  $\mathcal{S}$  to slide over itself (if doing so improves equilibrium) but penalizes drift in the normal direction. The third term, weaker than the second, regularizes the optimization by preventing large drift away from the reference surface or excessive tangential sliding.

**Implementation Details.** Solving the weighted least-squares problem of Step 3 amounts to solving a sparse, symmetric linear system. While the MINRES algorithm [Paige and Saunders 1975] is likely the most robust algorithm for solving this system, in practice we have observed that the method of conjugate gradients works

well despite the potential ill-conditioning of the objective matrix.

**Limitations.** This algorithm is not guaranteed to always converge; this fact is not surprising from the physics of the problem (if the boundary of the reference mesh encloses too large of a region,  $w_{\max}$  is set too low, and the density of the surface too high, a thrust network in equilibrium simply does not exist – the vault is too ambitious and cannot be built to stand; pillars are needed.)

We can, however, make a few remarks. Step 2 always decreases the equilibrium energy  $E$  of Equation (7) and Step 3 does as well as  $\beta \rightarrow 0$ . Moreover, as  $\alpha \rightarrow 0$  and  $\beta \rightarrow 0$ , Step 3 approaches a linear system with as many equations as unknowns; if this system has full rank, its solution sets  $E = 0$ . These facts suggest that the algorithm should generally converge to a thrust network in equilibrium, provided that Step 1 does not increase the loads by too much at every iteration, and this is indeed what we observe in practice. One case where this assumption is guaranteed to hold is if the thickness of the surface is allowed to freely vary, so that it can be chosen so that the surface has uniform density over the top view.

If the linear system in Step 3 is singular and infeasible, the algorithm can stall at  $E > 0$ . This failure occurs, for instance, when an interior vertex has height  $z_i$  lower than all of its neighbors, and Step 2 assigns all incident edges to that vertex a weight of zero: clearly no amount of moving the vertex or its neighbors can bring the vertex into equilibrium. We avoid such degenerate configurations by bounding weights slightly away from zero in (8), trading increased robustness for slight smoothing of the resulting surface. Attempting to optimize meshes that have self-intersecting top views (i.e., aren’t height fields), have too many impossible features, or are insufficiently supported by fixed boundary points can also result in errors and instability.

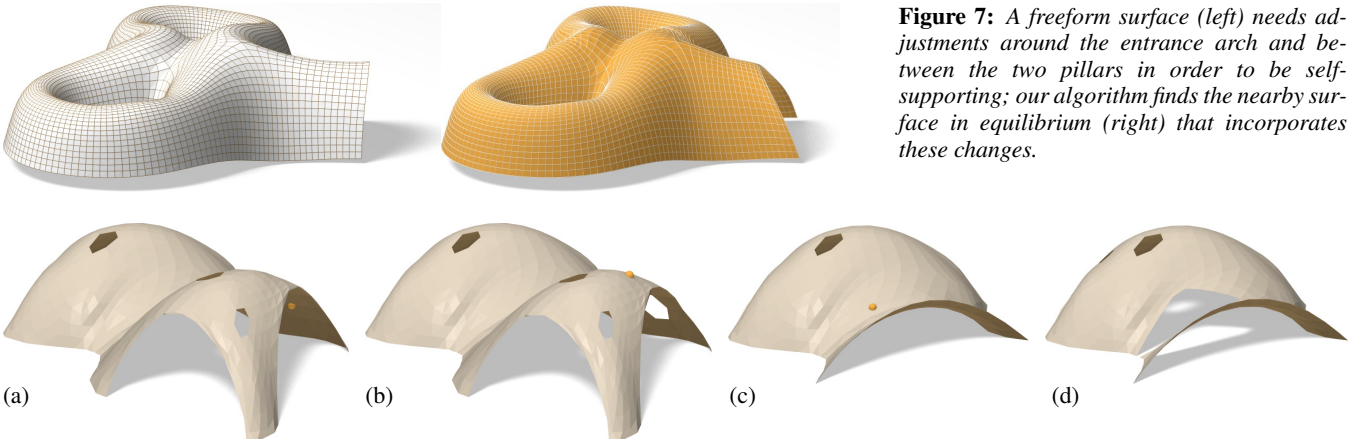


**Figure 8:** Destruction sequence. We simulate removing small parts of masonry (their location is shown by a yellow ball) and the falling off of further pieces which are no longer supported after removal. For this example, removing a certain small number of single bricks does not affect stability (a,b). Removal of material at a certain point (yellow) will cause a greater part of the structure to collapse, as seen in (c). (d) shows the result after one more removal (all images show the respective thrust networks, not the reference surface).

## 4 Results

**Interactive Design of Self-Supporting Surfaces.** The optimization algorithm described in the previous section forms the basis of an interactive design tool for self-supporting surfaces. Users manipulate a mesh representing a reference surface, and the computer searches for a nearby thrust network in equilibrium (see e.g. Figure 6). Features of the design tool include:

- Handle-based 3D editing of the reference mesh using Laplacian coordinates [Lipman et al. 2004; Sorkine et al. 2003] to extrude vaults, insert pillars, and apply other deformations to the reference mesh. Handle-based adjustments of the heights, keeping the top view fixed, and deformation of the top view, keeping the heights fixed, are also supported. The thrust network adjusts interactively to fit the deformed positions, giving the usual visual feedback about the effects of edits on whether or not the surface can stand.
- Specification of boundary conditions. Points of contact between the reference surface and the ground or environment are specified by “pinning” vertices of the surface, specifying that the thrust network must coincide with the reference mesh at this point, and relaxing the condition that forces must be in equilibrium there.
- Interactive adjustment of surface density  $\rho$ , external loads, and maximum permissible stress per edge  $w_{\max}$ , with visual feedback of how these parameters affect the fitted thrust network.
- Upsampling of the thrust network through Catmull-Clark subdivision and polishing of the resulting refined thrust network using optimization (§3).
- Visualization of the stress surface dual to the thrust network and corresponding reciprocal diagram.

**Example: Vault with Pillars.** As an example of the design and optimization workflow, consider a rectangular vault with six pillars, free boundary conditions along one edge, fixed boundary conditions along the others, and a tower extruded from the top of the surface (see Figure 6). This surface is neither convex nor simply connected, and exhibits a mix of boundary conditions, none of which cause our algorithm any difficulty; it finds a self-supporting thrust network near the designed reference mesh. The user is now free to make edits to the reference mesh, and the thrust network adapts to

these edits, providing the user feedback on whether these designs are physically realizable.

**Example: Top of the Lilium Tower.** Consider the top portion of the steel-glass exterior surface of the Lilium Tower, which is currently being built in Warsaw (see Figure 5). This surface contains a concave part with local minimum in its interior and so cannot possibly be self-supporting. Given this surface as a reference mesh, our algorithm constructs a nearby thrust network in equilibrium without the impossible feature. The user can then explore how editing the reference mesh – adding a pillar, for example – affects the thrust network and its deviation from the reference surface.

**Example: Freeform Structure with Two Pillars.** Suppose an architect’s experience and intuition has permitted the design of a nearly self-supporting freeform surface (Figure 7). Our algorithm reveals those edits needed to make the structure sound – principally around the entrance arch, and the area between the two pillars.

**Example: Destruction Sequence.** In Figure 8 we simulate removing parts of masonry and the falling off of further pieces which are no longer supported after removal. This is done by deleting the 1-neighborhood of a vertex and solving for a new thrust network in compressive equilibrium close to the original reference surface. We delete those parts of the network which deviate too much and are no longer contained in the masonry hull, and iterate.

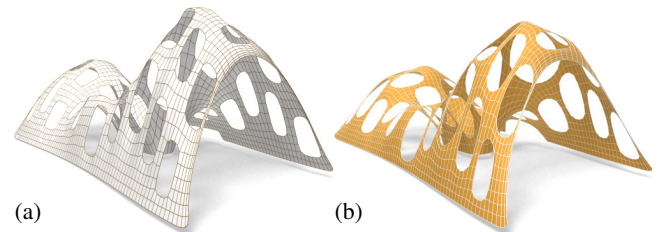


**Figure 9:** A mesh with holes (a) requires large deformations to both the top view and heights to render it self-supporting (b)

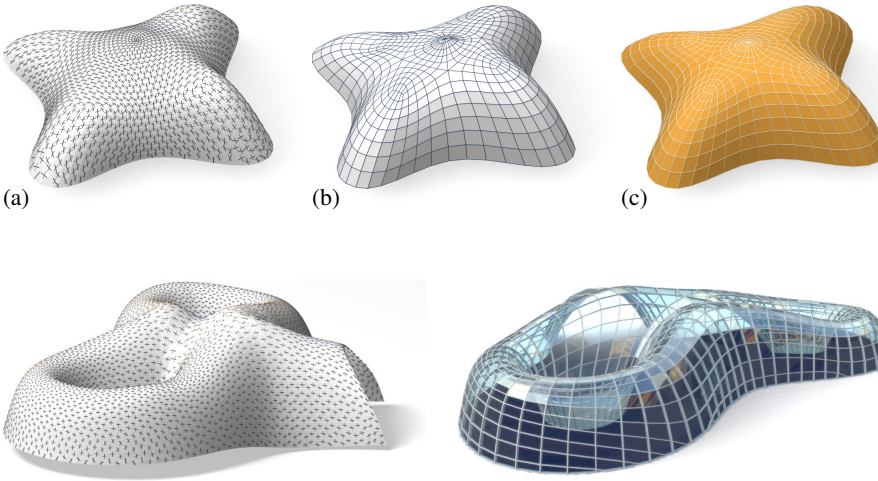


**Figure 11:** Planar quad remeshing of the surface of Figure 7. Left: Principal directions. Center: The result of optimization is a self-supporting PQ mesh, which guides a moment-free steel/glass construction. Right: Interior view.

**Example: Swiss Cheese.** Cutting holes in a self-supporting surface interrupts force flow lines and causes dramatic global changes to the surface stresses, often to the point that the surface is no longer in equilibrium. Whether a given surface with many such holes can stand is far from obvious. Figure 9 shows such an implausible and unstable surface; our optimization finds a nearby, equally implausible but stable surface without difficulty (see Figures 1 and 9).

which approximates a given continuous surface  $s(x, y)$ . It is known that  $\mathcal{S}$  must approximately follow a network of conjugate curves in the surface (see e.g. [Liu et al. 2006]). We can derive this condition in an elementary way as follows: Using a Taylor expansion, we compute the volume of the convex hull of the quadrilateral  $\mathbf{v}_{ij}, \mathbf{v}_{i+1,j}, \mathbf{v}_{i+1,j+1}, \mathbf{v}_{i,j+1}$ , assuming the vertices lie exactly on the surface  $s(x, y)$ . This results in

$$\text{vol} = \frac{1}{6} \det(\mathbf{a}_1, \mathbf{a}_2) \cdot ((\mathbf{a}_1)^T \nabla^2 s \mathbf{a}_2) + \dots,$$

$$\text{where } \mathbf{a}_1 = \begin{pmatrix} x_{i+1,j} - x_{i,j} \\ y_{i+1,j} - y_{i,j} \end{pmatrix}, \quad \mathbf{a}_2 = \begin{pmatrix} x_{i,j+1} - x_{i,j} \\ y_{i,j+1} - y_{i,j} \end{pmatrix},$$

and the dots indicate higher order terms. We see that planarity requires  $(\mathbf{a}_1)^T \nabla^2 s \mathbf{a}_2 = 0$ . In addition to the mesh  $\mathcal{S}$  approximating the surface  $s(x, y)$ , the corresponding polyhedral Airy surface  $\Phi$  must approximate  $\phi(x, y)$ ; thus we get the conditions

$$(\mathbf{a}_1)^T \nabla^2 s \mathbf{a}_2 = (\mathbf{a}_1)^T \nabla^2 \phi \mathbf{a}_2 = 0.$$

$\mathbf{a}_1, \mathbf{a}_2$  are therefore eigenvectors of  $(\nabla^2\phi)^{-1}\nabla^2s$ . In view of §2.3,  $\mathbf{a}_1, \mathbf{a}_2$  indicate the principal directions of the surface  $s(x, y)$  relative to  $\phi(x, y)$ .

In the discrete case, where  $s, \phi$  are not given as continuous surfaces, but are represented by a mesh in equilibrium and its Airy mesh, we use the techniques of Schiftner [2007] and Cohen-Steiner and Morvan [2003] to approximate the Hessians  $\nabla^2 s, \nabla^2 \phi$ , compute principal directions as eigenvectors of  $(\nabla^2\phi)^{-1}\nabla^2s$ , and subsequently find meshes  $\mathcal{S}, \Phi$  approximating  $s, \phi$  which follow those directions. Global optimization can now polish  $\mathcal{S}, \Phi$  to a valid thrust network with discrete stress potential, where before it failed: we do so by taking the planarity energy  $\sum_f (2\pi - \theta_f)^2$ , where the sum runs over faces and  $\theta_f$  is the sum of the interior angles of face  $f$ , linearizing it at every iterations, and adding it to the objective function of the position update (Step 3). Convexity of  $\Phi$  ensures that  $\mathcal{S}$  is self-supporting.

Note that for each  $\Phi$ , the relative principal curvature directions give the *unique* curve network along which a planar quad discretization of a self-supporting surface is possible. Other networks lead to results like the one shown by Figure 12. Figures 10 and 11 further illustrate the result of applying this procedure to self-supporting surfaces.

*Remark:* When remeshing a given shape by planar quad meshes, we know that the circular and conical properties require that the mesh

## 5 Special Self-Supporting Surfaces

**PQ Meshes.** Meshes with *planar* faces are of particular interest in architecture, so in this section we discuss how to remesh a given thrust network in equilibrium such that it becomes a quad mesh with planar faces (again in equilibrium). If this mesh is realized as a steel-glass construction, it is self-supporting in its beams alone, with no forces exerted on the glass (this is the usual manner of using glass). The beams constitute a self-supporting structure which is in perfect force equilibrium (without moments in the nodes) if only the deadload is applied.

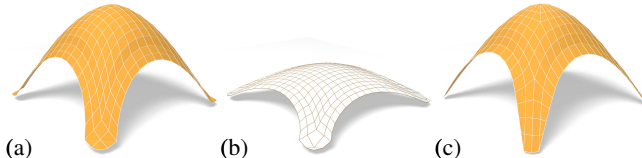


**Figure 12:** Directly enforcing planarity of the faces of even a very simple self-supporting quad-mesh vault (a) results in a surface far removed from the original design (b). Starting instead from a remeshing of the surface with edges following relative principal curvature directions yields a self-supporting, PQ mesh far more faithful to the original (c).

Taking an arbitrary non-planar quad mesh and attempting naive, simultaneous enforcement of planarity and static equilibrium – either by staggering a planarity optimization step every outer iteration, or adding a planarity penalty term to the position update – does not yield good results, as shown in Figure 12. Indeed, as we will see later in this section, such a planar perturbation of a thrust network is not expected to generally exist.

Consider a planar quad mesh  $\mathcal{S}$  with vertices  $\mathbf{v}_{ij} = (x_{ij}, y_{ij}, s_{ij})$

**Figure 10:** Planar quad remeshing of the “Lilium tower” surface of Figure 5. (a) Principal directions which are found as eigenvectors of  $(\nabla^2\phi)^{-1}\nabla^2s$ . (b) Quad mesh guided by principal directions is almost planar and almost self-supporting. (c) Small changes achieve both properties.



follows the ordinary, Euclidean principal curvature directions [Liu et al. 2006]. It is remarkable that the self-supporting property in a similar manner requires us to follow certain *relative* principal directions. Practitioners' observations regarding the beneficial statics properties of principal directions can be explained by this analogy, because the relative principal directions are close to the Euclidean ones, if the stress distribution is uniform and  $\|\nabla s\|$  is small.

**Koenigs Meshes.** Given a self-supporting thrust network  $\mathcal{S}$  with stress surface  $\Phi$ , we ask the question: Which vertical perturbation  $\mathcal{S} + \mathcal{R}$  is self-supporting, with the same loads as  $\mathcal{S}$ ? As to notation, all involved meshes  $\mathcal{S}, \mathcal{R}, \Phi$  have the same top view, and arithmetic operations refer to the respective  $z$  coordinates  $s_i, r_i, \phi_i$  of vertices.

The condition of equal loads then is expressed as  $\Delta_\phi(s + r) = \Delta_\phi s$  in terms of Laplacians or as  $H_{\mathcal{S}}^{\text{rel}} = H_{\mathcal{S} + \mathcal{R}}^{\text{rel}}$  in terms of mean curvature, and is equivalent to

$$\Delta_\phi r = 0, \quad \text{i.e.,} \quad H_{\mathcal{R}}^{\text{rel}} = 0.$$

So  $\mathcal{R}$  is a *minimal surface* relative to  $\Phi$ . While in the triangle mesh case there are enough degrees of freedom for nontrivial solutions, the case of planar quad meshes is more intricate: Polar polyhedra  $\mathcal{R}^*, \Phi^*$  have to be Christoffel duals of each other [Pottmann and Liu 2007], as illustrated by Figure 4. Unfortunately not all quad meshes have such a dual; the condition is that the mesh is *Koenigs*, i.e., the derived mesh formed by the intersection points of diagonals of faces again has planar faces [Bobenko and Suris 2008].



**Figure 13:** A “Koebe” mesh  $\Phi$  is self-supporting for unit dead load. An entire family of self-supporting meshes with the same top view is defined by  $\mathcal{S}_\alpha = \Phi + \alpha\mathcal{R}$ , where  $\mathcal{R}$  is chosen as  $\Phi$ 's Christoffel-dual.

**Koebe meshes.** An interesting special case occurs if  $\Phi$  is a *Koebe mesh* of isotropic geometry, i.e., a PQ mesh whose edges touch the Maxwell paraboloid. Since  $\Phi$  approximates the Maxwell paraboloid, we get  $2K(\mathbf{v}_i)H^{\text{rel}}(\mathbf{v}_i) \approx 1$  and  $\Phi$  consequently is self-supporting for unit load. Applying the Christoffel dual construction described above yields a minimal mesh  $\mathcal{R}$  and a family of meshes  $\Phi + \alpha\mathcal{R}$  which are self-supporting for unit load (see Figure 13).

## 6 Conclusion and Future Work

**Conclusion.** This paper builds on relations between statics and geometry, some of which have been known for a long time, and connects them with newer methods of discrete differential geometry, such as discrete Laplace operators and curvatures of polyhedral surfaces. We were able to find efficient ways of modeling self-supporting freeform shapes, and provide architects and engineers with an interactive tool for evaluating the statics of freeform geometries. The self-supporting property of a shape is directly relevant for freeform masonry. The actual thrust networks we use for computation are relevant e.g. for steel constructions, where equilibrium of deadload forces implies absence of moments. This theory and accompanying algorithms thus constitute a new contribution to architectural geometry, connecting statics and geometric design.

**Future Work.** There are several directions of future research. One is to incorporate non-manifold meshes, which occur naturally when e.g. supporting walls are introduced. It is also obvious that non-vertical loads, e.g. wind load, play a role. There are also some directions to pursue in improving the algorithms, for instance adaptive remeshing in problem areas. Probably the interesting connections between statics properties and geometry are not yet exhausted, and we would like to propose the *geometrization* of problems as a strategy for their solution.

**Acknowledgements.** This work was very much inspired by Philippe Block's plenary lecture at the 2011 Symposium on Geometry Processing in Lausanne. Several illustrations (the maximum load example of Figure 14 and the destruction sequence of Figure 8) have real-world analogues on his web page [Block 2011].

## References

- ANDREU, A., GIL, L., AND ROCA, P. 2007. Computational analysis of masonry structures with a funicular model. *J. Engrg. Mechanics* 133, 473–480.
- ASH, P., BOLKER, E., CRAPO, H., AND WHITELEY, W. 1988. Convex polyhedra, Dirichlet tessellations, and spider webs. In *Shaping space (Northampton 1984)*. Birkhäuser, 231–250.
- BARNES, M. R. 2009. Form finding and analysis of tension structures by dynamic relaxation. *Int. J. Space Structures* 14, 2, 89–104.
- BLOCK, P., AND LACHAUER, L. 2011. Closest-fit, compression-only solutions for free form shells. In *IABSE — IASS 2011 London Symposium*, Int. Ass. Shell Spatial Structures. electronic.
- BLOCK, P., AND OCHSENDORF, J. 2007. Thrust network analysis: A new methodology for three-dimensional equilibrium. *J. Int. Assoc. Shell and Spatial Structures* 48, 3, 167–173.
- BLOCK, P. 2009. *Thrust Network Analysis: Exploring Three-dimensional Equilibrium*. PhD thesis, Massachusetts Institute of Technology.
- BLOCK, P., 2011. Project webpage at <http://block.arch.ethz.ch/projects/freeform-catalan-thin-tile-vaulting>.
- BOBENKO, A., AND SURIS, YU. 2008. *Discrete differential geometry: Integrable Structure*. No. 98 in Graduate Studies in Math. American Math. Soc.
- BOBENKO, A., POTTMANN, H., AND WALLNER, J. 2010. A curvature theory for discrete surfaces based on mesh parallelity. *Math. Annalen* 348, 1–24.
- COHEN-STEINER, D., AND MORVAN, J.-M. 2003. Restricted Delaunay triangulations and normal cycle. In *Proc. 19th Symp. Computational geometry*, ACM, 312–321.
- FRATERNALI, F., ANGELILLO, M., AND FORTUNATO, A. 2002. A lumped stress method for plane elastic problems and the discrete-continuum approximation. *Int. J. Solids Struct.* 39, 6211–6240.
- FRATERNALI, F. 2010. A thrust network approach to the equilibrium problem of unreinforced masonry vaults via polyhedral stress functions. *Mechanics Res. Comm.* 37, 2, 198 – 204.
- FRIEDLANDER, M. P., 2007. BCLS: Bound constrained least squares. <http://www.cs.ubc.ca/~mpf/bcls>.

- 692 GIAQUINTA, M., AND GIUSTI, E. 1985. Researches on the equi-  
693 librium of masonry structures. *Archive for Rational Mechanics*  
694 and *Analysis* 88, 4, 359–392.
- 695 GLYMPH, J., SHELDEN, D., CECCATO, C., MUSSEL, J., AND  
696 SCHOBER, H. 2004. A parametric strategy for free-form glass  
697 structures using quadrilateral planar facets. *Automation in Con-  
698 struction* 13, 2, 187 – 202.
- 699 HEYMAN, J. 1966. The stone skeleton. *Int. J. Solids Structures* 2,  
700 249–279.
- 701 HEYMAN, J. 1995. *The Stone Skeleton: Structural Engineering of  
702 Masonry Architecture*. Cambridge University Press.
- 703 HEYMAN, J. 1998. *Structural Analysis: A Historical Approach*.  
704 Cambridge University Press.
- 705 KILIAN, A., AND OCHSENDORF, J. 2005. Particle-spring sys-  
706 tems for structural form finding. *J. Int. Assoc. Shell and Spatial  
707 Structures* 46, 77–84.
- 708 LIPMAN, Y., SORKINE, O., COHEN-OR, D., LEVIN, D., ROSSI,  
709 C., AND SEIDEL, H. 2004. Differential coordinates for interac-  
710 tive mesh editing. In *Proc. SMI*. IEEE, 181–190.
- 711 LIU, Y., POTTMANN, H., WALLNER, J., YANG, Y.-L., AND  
712 WANG, W. 2006. Geometric modeling with conical meshes  
713 and developable surfaces. *ACM Trans. Graph.* 25, 3, 681–689.
- 714 LIVESLEY, R. K. 1992. A computational model for the limit anal-  
715 ysis of three-dimensional masonry structures. *Meccanica* 27,  
716 161–172.
- 717 MAXWELL, J. 1864. On reciprocal diagrams and diagrams of  
718 forces. *Philosophical Magazine* 4, 27, 250–261.
- 719 O'Dwyer, D. 1998. Funicular analysis of masonry vaults. *Com-  
720 puters and Structures* 73, 187–197.
- 721 PAIGE, C. C., AND SAUNDERS, M. A. 1975. Solution of sparse  
722 indefinite systems of linear equations. *SIAM J. Num. Analysis*  
723 12, 617–629.
- 724 POTTMANN, H., AND LIU, Y. 2007. Discrete surfaces in isotropic  
725 geometry. In *Mathematics of Surfaces XII*, M. Sabin and J. Win-  
726 kler, Eds., vol. 4647 of *LNCS*. Springer-Verlag, 341–363.
- 727 POTTMANN, H., LIU, Y., WALLNER, J., BOBENKO, A., AND  
728 WANG, W. 2007. Geometry of multi-layer freeform structures  
729 for architecture. *ACM Trans. Graphics* 26, 3, #65,1–11.
- 730 SCHIFTNER, A., AND BALZER, J. 2010. Statics-sensitive layout  
731 of planar quadrilateral meshes. In *Advances in Architectural Ge-  
732 ometry 2010*, C. Ceccato et al., Eds. Springer, Vienna, 221–236.
- 733 SCHIFTNER, A. 2007. *Planar quad meshes from relative principal  
734 curvature lines*. Master's thesis, TU Wien.
- 735 SORKINE, O., COHEN-OR, D., AND TOLEDO, S. 2003. High-  
736 pass quantization for mesh encoding. In *Symposium Geometry  
737 processing*. Eurographics Assoc., 42–51.
- 738 VAN MELE, T., AND BLOCK, P. 2011. A novel form finding  
739 method for fabric formwork for concrete shells. *J. Int. Assoc.  
740 Shell and Spatial Structures* 52, 217–224.
- 741 WARDETZKY, M., MATHUR, S., KÄLBERER, F., AND GRIN-  
742 SPUN, E. 2007. Discrete Laplace operators: No free lunch.  
743 In *Symposium on Geometry Processing*. 33–37.
- 744 WHITING, E., OCHSENDORF, J., AND DURAND, F. 2009. Pro-  
745 cedural modeling of structurally-sound masonry buildings. *ACM  
746 Trans. Graph.* 28, 5, #112,1–9.

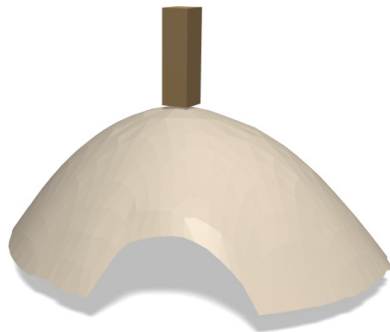


**Figure 14:** Testing stability. This self-supporting surface of length 24 m is imagined as masonry of thickness 0.1 m. It possesses a thrust network inside the masonry hull if – for the sake of example – a load of 11.000 kg (shown in dark) is applied to a certain vertex. This means that the surface is still stable after that load is applied (N.B. This method of testing is rather conservative).

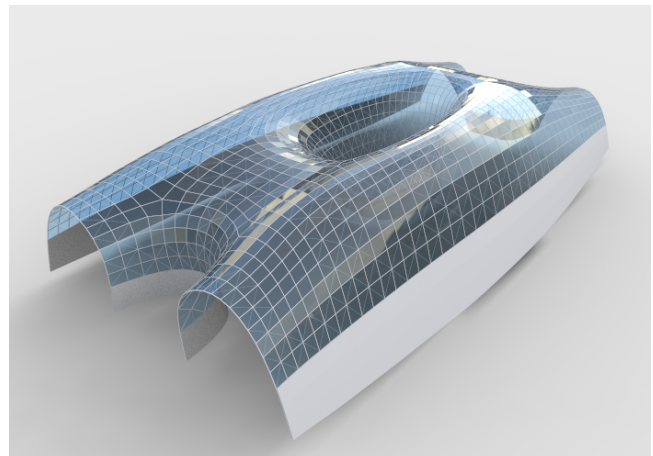


**Figure 15:** Glass as a structural element can support stresses up to, say, 30 MPa. We propose a steel/glass construction which utilizes the structural properties of glass by first solving for a self-sup-  
porting thrust network such that forces do not exceed the maximum values, and subsequent remeshing of this surface by a planar quad mesh (not necessarily self-supporting itself). Since this surface is very close to a self-supporting shape, joints will experience low bending and torsion moments.